Supplementary Information for

Mimic Metalloenzymes with Atomically Dispersed Fe Sites into Covalent Organic Framework Membranes for Enhanced CO_2 Photoreduction

Shuaiqi Gao,[1] Xiao Zhao,[2] Qian Zhang,[1] Linlin Guo,[1] Zhiyong Li,[1] Huiyong Wang,[1]* Suojiang Zhang[3,4], and Jianji Wang[1]*

[1] Key Laboratory of Green Chemical Media and Reactions (Ministry of Education), Collaborative Innovation Center of Henan Province for Green Manufacturing of Fine Chemicals, School of Chemistry and Chemical Engineering, Henan Normal University, Xinxiang, Henan 453007, P. R. China.

[2] Science and Technology on Aerospace Chemical Power Laboratory, Hubei Institute of Aerospace Chemotechnology, Xiangyang, 441003, P. R. China.

[3] College of Chemistry and Molecular Sciences, Longzihu New Energy Laboratory, Henan University, Zhengzhou, Henan 450000, P. R. China.

[4] Beijing Key Laboratory of Ionic Liquids Clean Process, State Key Laboratory of Multiphase Complex Systems, Institute of Process Engineering, Chinese Academy of Sciences, Beijing 100190, P. R. China.

*Correspondence author. Email: hywang@htu.edu.cn (H.Y.W), jwang@htu.edu.cn (J.J.W).

Table of Contents

1. Experimental section

1.1 Materials and chemicals

2,4,6-Tris(4-formylphenyl)-1,3,5-triazine (TTB, 98%, Yanshen, China), 2,4,6-tris(4-aminophenyl)-1,3,5-triazine (TAPT, 98%, Yanshen, China), $FeCl_2$ (98%, Macklin) and p-toluenesulfonic acid (PTSA, 98%, Aladdin) were used directly in the synthetic experiments. Nylon microfiltration membrane with an average pore size of 0.2 μm were purchased from Tianjin Jinteng Filtration Co., Ltd. Ar gas (99.99%) and $^{12}CO_2$ gas (99.999%) were purchased from Yuxin Gas Manufacturing Co., Ltd (Xinxiang, China). Labeling $^{13}CO_2$ gas was purchased from Sigma Aldrich Co., Ltd (enrichment, 99 at.%, and chemical purity, 99.9%).

1.2 Synthesis of 1-decyl-3-methylimidazolium bis(trifluoromethanesulphonyl) imide ionic liquid

1-Decyl-3-methylimidazolium bis(triuoromethylsulfonyl)imide ($[C_{10}Mim][Tf_2N]$) ionic liquid was prepared and purified by using the procedures described in the literature[1]. Briefly, aqueous lithium bis(trifluoromethanesulphonyl)imide (22.39 g, 0.078 mol) was added dropwise to a cooled aqueous solution (200 mL) of 1-decyl-3-methylimidazolium chloride (20.2 g, 0.078 mol) under stirring. The bottom ionic liquid layer was collected via a separating funnel, dissolved in dichloromethane (300 mL), and washed with water (2 × 150 mL). The organic layer was collected and dried over anhydrous $MgSO_4$. After filtration, the solvent was removed under reduced pressure to yield the light yellow liquid as $[C_{10}Mim][Tf_2N]$.

1.3 Synthesis of COF membrane

The reaction between TTB (2,4,6-tris(4-formylphenyl)-1,3,5-triazine) and TAPT (2,4,6-Tris(4-aminophenyl)-1,3,5-triazine) was performed at ionic liquid-H_2O interface. Firstly, 15.73 mg of TTB was dissolved in 20 mL the ionic liquid to give a 2 mmol/L solution of aldehyde (A). Then, 2 m mmol/L aqueous solution of amine (B) was prepared by dissolving 14.17 mg TAPT in 20 mL water and adding 15.2 mg p-toluenesulfonic acid as the catalyst. After that, 2 mL A solution was transferred to a 20 mL culture bottle, and 6 mL water was added on the top of the A solution to form a

spacer layer of water. Thereafter, 2 mL B solution was added slowly to the top of the spacer layer in 2 min. The above system was kept at room temperature under undisturbed conditions for 120 h to obtain COF membranes. The membrane formed at the interface was collected and washed thoroughly with dichloromethane, DMF and ethanol in turn, and put aside for further investigations.

1.4 Synthesis of Fe-COF membrane

A COF membrane was placed in 10 mL methanol solution with different weights of $FeCl_2$ and heating reflux at 60 °C for 8 hours under the N_2 atmosphere. Then the COF membrane is washed with water and methanol to obtain the Fe-COF membrane.

1.5 Materials Characterization

X-ray diffraction (XRD) patterns were collected on an X-ray diffractometer (X' Pert3 Powder) equipped with a Kratky block-collimation system at 25.0 ± 0.1 °C and a sealed-tube X-ray generator with the Cu target operating at 45 kV and 40 mA. Nitrogen adsorption and desorption isotherms were measured at 77 K on a Quantachrome Autosorb-iQ adsorption analyzer, and the samples were degassed under vacuum at 250 °C for analysis. Specific surface areas and pore size distributions were obtained by the Brunauer-Emmet-Teller (BET) model and the nonlocal density functional theory (NLDFT) model, respectively. CO_2 adsorption isotherms were measured at 25 °C by using a Quantachrome Autosorb-iQ adsorption analyzer after the degassing process at 200 °C for 12 h. Transmission electron microscopy (TEM) images were recorded on the FEI Talos F200X electron microscopy. The X-ray photoelectron spectrum (XPS) was recorded on a Thermo Scientific K-Alpha electron energy spectrometer using Al Kα (1486.6 eV) radiation as the X-ray excitation source. Scanning electron microscope (SEM) patterns were obtained on a JEOL JSM-6390LV microscope. Fourier transform infrared (FTIR) spectra were determined by using a Spectrum 400F infrared spectrometer. Electrochemical tests were carried out on the CHI 760E electrochemical working station (Shanghai). The photoluminescence (PL) and time-resolved fluorescence decay spectra (TRFL) were measured on the FLS980 fluorescence spectrometers (UK). Solid-state UV-vis diffuse reflectance spectra of different samples

were collected on a Perkin Elmer Lambda 950 spectrometer (USA) using $BaSO_4$ as the reference standard. Thermogravimetric analysis (TGA) was conducted from 25 ℃ to 800 ℃ under N_2 protection with a heating rate of 10 ℃ min^{-1} on a NETZSCH STA449C thermal analyzer. CO_2 temperature-programmed desorption (CO_2-TPD) was performed on an Autochem 2920 II chemisorption analyzer (Micromeritics) equipped with a thermal conductivity detector.

1.6 CO_2 photocatalytic reduction tests

Photocatalytic CO_2 reduction reaction to CO was performed in a 250 mL optical reaction reactor (PQ256, Beijing Perfectlight Technology Co., Ltd, China) under full light (320-780 nm) irradiation and stirring at 25 ºC. In the gas-phase reaction, 1.5 ± 0.5 mg of the membrane catalyst (with an area of 3.14 cm^2) was first dried under vacuum and then placed on the idiosyncratic reaction tripod (height is 3.5 cm). Next, 3 mL of distilled water was added to the bottom of the optical reaction reactor. Before the reaction, the reactor was evacuated by a vacuum pump followed by purging with high-purity CO_2 three times, and then CO_2 gas was bubbled through the reactor for 30 minutes to fill with 1 atm of humid CO_2. A 300 W xenon lamp (Beijing Perfectlight, Microsolar 300) was used as a light source, and the light intensity was standard sunlight (100 mW cm^{-2}). The photocatalytic CO_2 reduction measurement was conducted in an airtight online real-time test system with a Fuli 9790II Gas Chromatograph (Zhejiang, China), where 3 mL water was injected into the bottom of the photocatalytic reactor before sealing the system that ensured the water vapor was saturated during photocatalysis. At the same time, the liquid products were determined by ^1H NMR spectroscopy (Bruker AVIII HD 600). For the isotopic labeling experiment, $^{13}CO_2$ gas was employed to replace $^{12}CO_2$ gas as the carbon source and the gas products were analyzed by gas chromatography-mass spectrometry (GC-MS, Agilent GC/MS-7000D).

1.7 In-situ attenuated total reflectance (ATR) infrared spectrometric measurements

The in-situ ATR infrared spectrometric measurements were conducted by a Thermo Nicolet iS50 spectrometer (USA) with an MCT detector in the system. In a typical

procedure, the Fe-COF membrane was placed in the chamber before sealing and then purging with N_2 gas for 60 min. Typical signals of several intermediates were captured after the introduction of a flowing CO_2 (g) and H_2O (g) under dark for 10 min and then visible light irradiation for 0-60 min.

1.8 Photoelectrochemical measurements

Photoelectrochemical and electrochemical measurements including photocurrent, electrochemical impedance spectra (EIS), and Mott-Schottky plot were performed with an electrochemical working station (CHI 760E) via a three-electrode quartz cell. Catalyst samples were smeared on the ITO conductive plate to prepare the working electrode, while the Ag/AgCl electrode and Pt mesh were immersed in sodium sulfate aqueous solution (0.5 M) to serve as the reference electrode and the counter electrode, respectively. For photocurrent measurements, photoirradiation conditions were the same as photocatalytic tests. In the EIS measurements, the frequency limit was set at the range from 100 kHz to 0.01 Hz with 5 mV of voltage amplitude at the open-circuit potential. For Mott-Schottky plot measurements, the samples were tested with different frequencies at 500, 1000, and 1500 Hz.

1.9 Apparent quantum efficiency (AQE)

The AQE was measured under monochromatic lights with different wavelengths in an identical experimental setup and the same condition as the CO_2 photo-reduction test. In detail, the typical irradiated area of 3.14 cm^2 for 1.0 mg Fe-COF membrane was placed horizontally in the center of a 250 mL optical reaction reactor, and monochromatic lights with different wavelengths (420 nm, 450 nm, 530 nm, 550 nm, and 630 nm) were applied as incident light resources. The intensity of monochromatic light at each wavelength was calibrated by the photometer (Newport 91150-2000) placed at the identical position of the catalysts. The sample was irradiated for 1 hour at each wavelength and the photo-catalytic products were collected to analyze the yield. The AQE value was calculated as the number of electrons consumed to generate the product divided by the total number of incident photos (Equation 1)[2,3]. Each AQE measurement was repeated at least four times in parallel to obtain a reproducible and

reliable value.

$$\mathrm{AQE}(\%) = \frac{\text{Total consumed electron number}}{\text{number of incidented photons}} \times 100\% = \frac{2 \times M \times N_A \times h \times c}{S \times P \times t \times \lambda} \times 100\% \quad (1)$$

where M is the amount of CO (mol), N_A is Avogadro's constant (6.022×10^{23} mol^{-1}), h is Planck's constant (6.63×10^{-34} $J\cdot s^{-1}$), c is the speed of light (3×10^{8} $m\cdot s^{-1}$), P is irradiation intensity (W cm^{-2}), S is the irradiation area (cm^2), t is irradiation time (s), and λ is the wavelength of the light source (m), respectively.

2. DFT computational details

All DFT calculations were performed using the Vienna ab initio simulation package (VASP). The generalized gradient approximation (GGA) with the Perdew–Burke–Emzerhof (PBE) functional was employed to describe the exchange correlation energy. Projector augmented wave (PAW) methods were used for the pseudopotentials. The energy cutoff for the plane wave basis was set to be 500 eV, and the convergence criterion of geometry relaxation was 0.02 eV/Å in force. The Brillouin zones (BZ) were sampled with 2 × 2 × 1 K points. For geometric optimization, the convergence criteria for energy were set to 1×10^{-5} eV. Also, the optimized structures were then used to calculate the electronic structures. A vacuum of 20 Å added along the direction normal to the atomic slab was built for the calculations. The free energy diagrams for the CO_2 photoreduction pathway are calculated through the VASPKIT tool based on the equation ($\Delta G = \Delta E + \Delta E_{ZPE} - T\Delta S$), where ΔE, ΔE_{ZPE}, and $T\Delta S$ represent the calculated electronic energy, zero-point energy, and entropy contribution, respectively.

3. Figures S1-S23

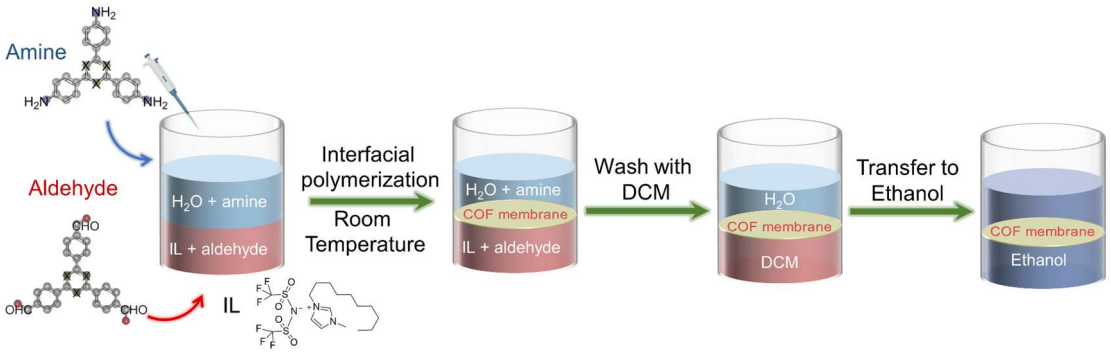

Fig. S1. The fabrication process of the COF membranes via interfacial reaction. Note: Aldehyde in ionic liquid and amine/PTSA (catalyst) in water were designed for the synthesis of the COF membranes at the interface of ionic liquid-H_2O.

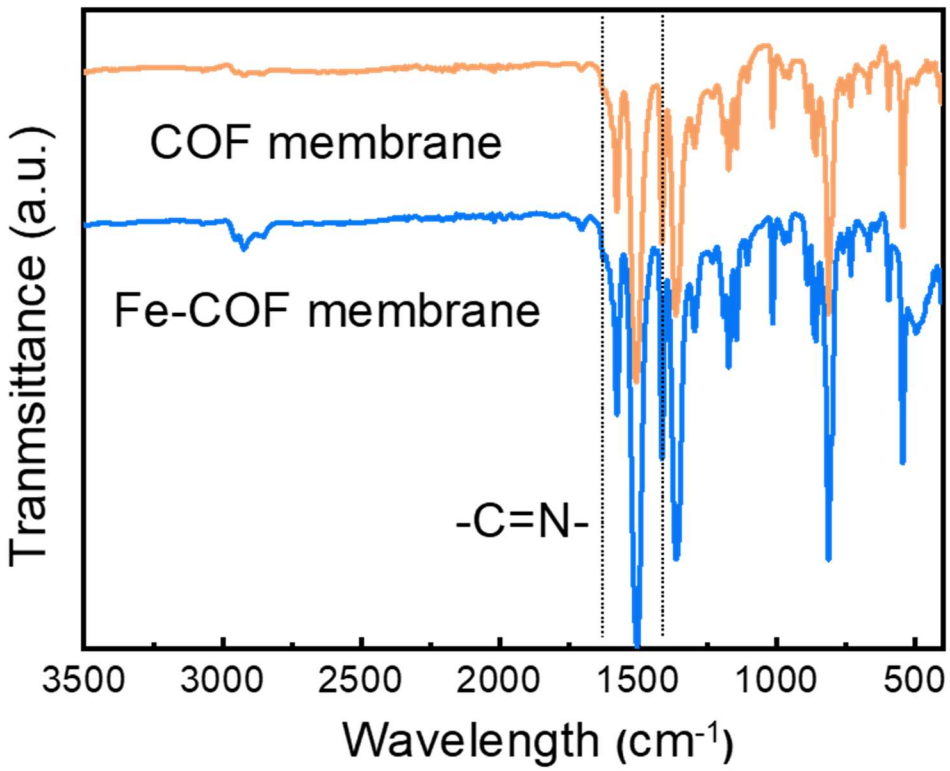

Fig. S2. FTIR spectra of different COF membranes.

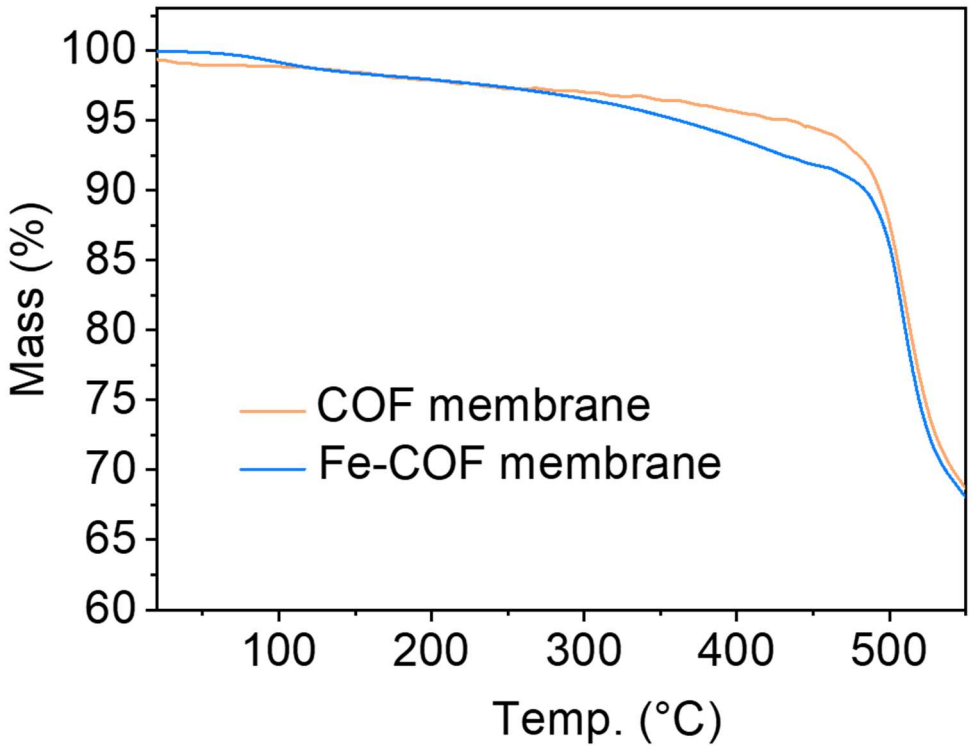

Fig. S3. TGA curves of different COF membranes.

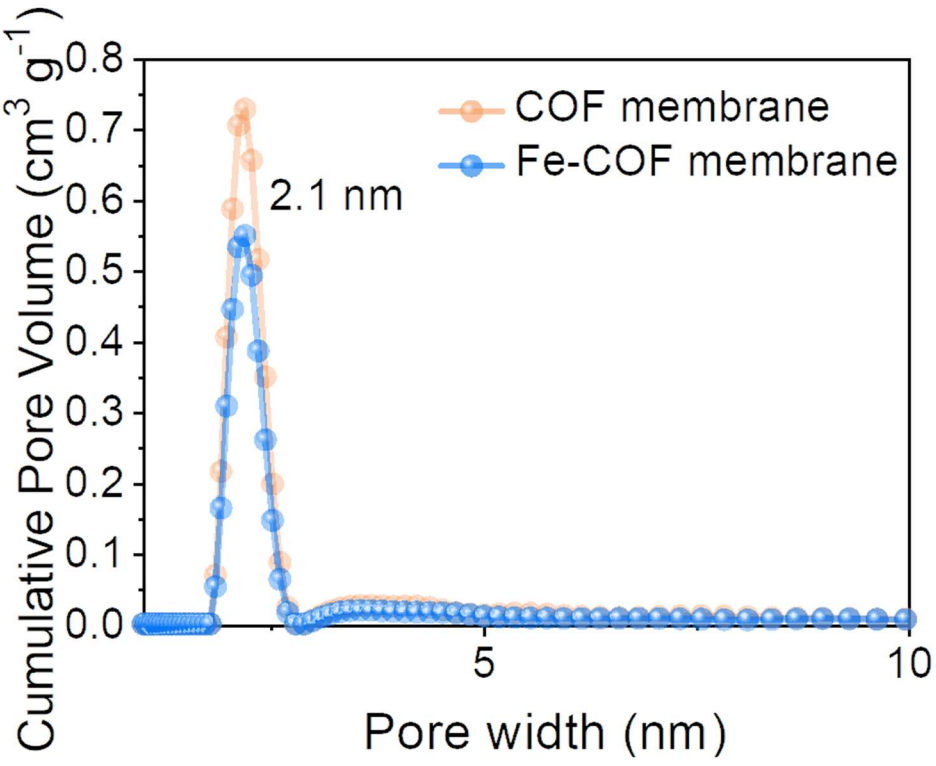

Fig. S4. The pore size distribution of different COF membranes.

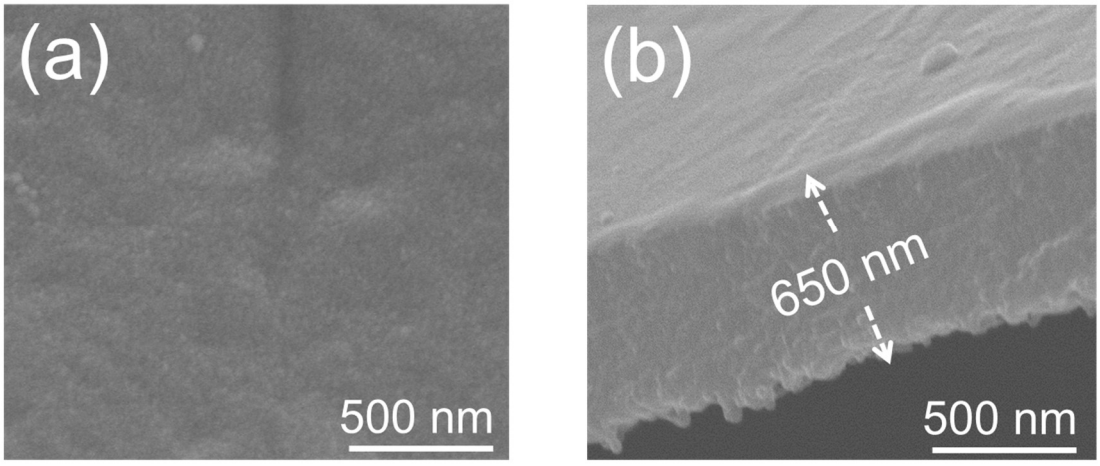

Fig. S5. SEM images of the pristine COF membrane.

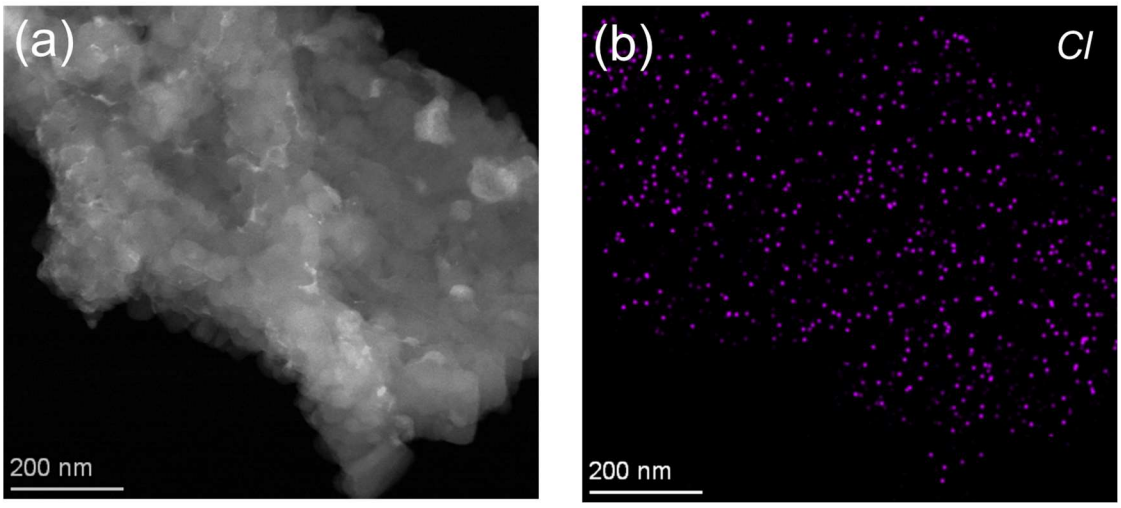

Fig. S6. (a) TEM images and (b) element mapping of the Fe-COF membrane.

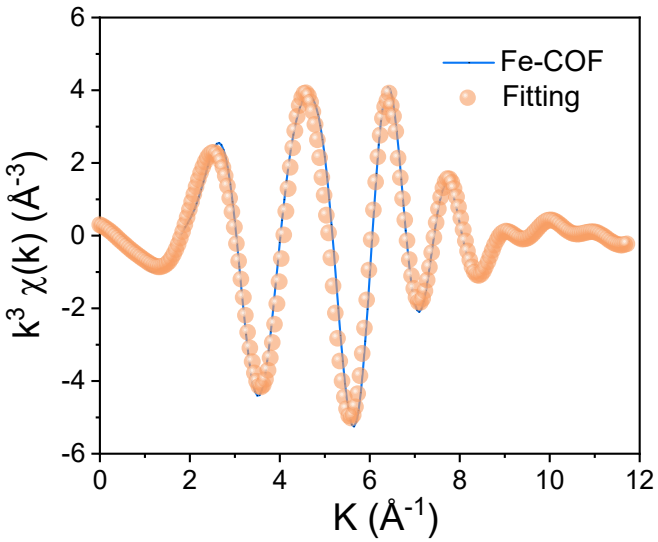

Fig. S7. EXAFS fitting curves of the Fe-COF membrane at q space.

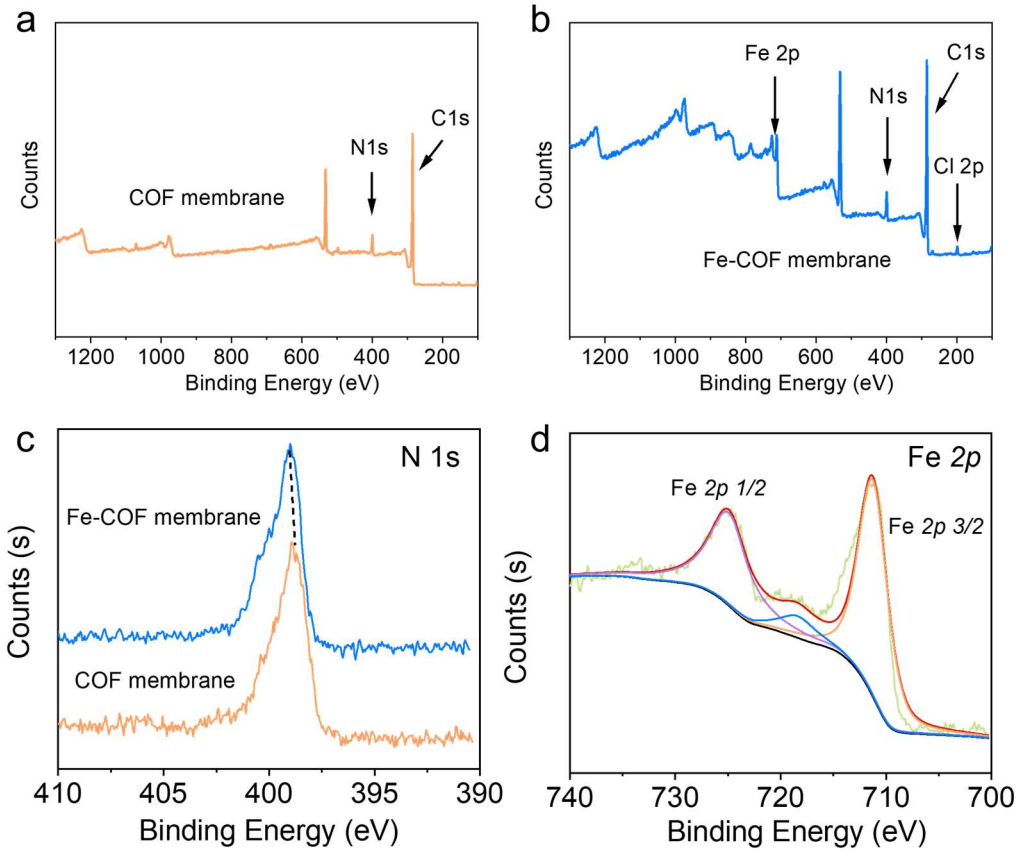

Fig. S8. XPS spectra of different COF membranes. (a-b) XPS survey spectra and (c-d) high-resolution XPS spectra.

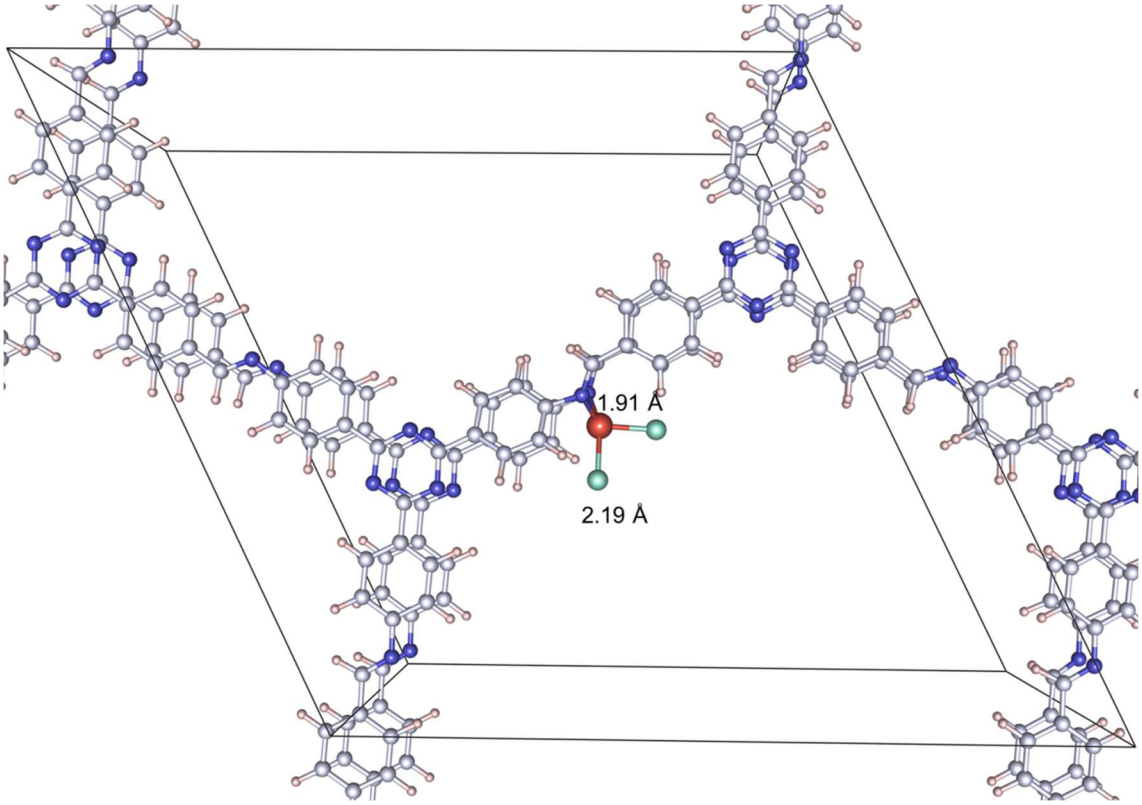

Fig. S9. The optimized local atomic structure model of the Fe-COF membrane.

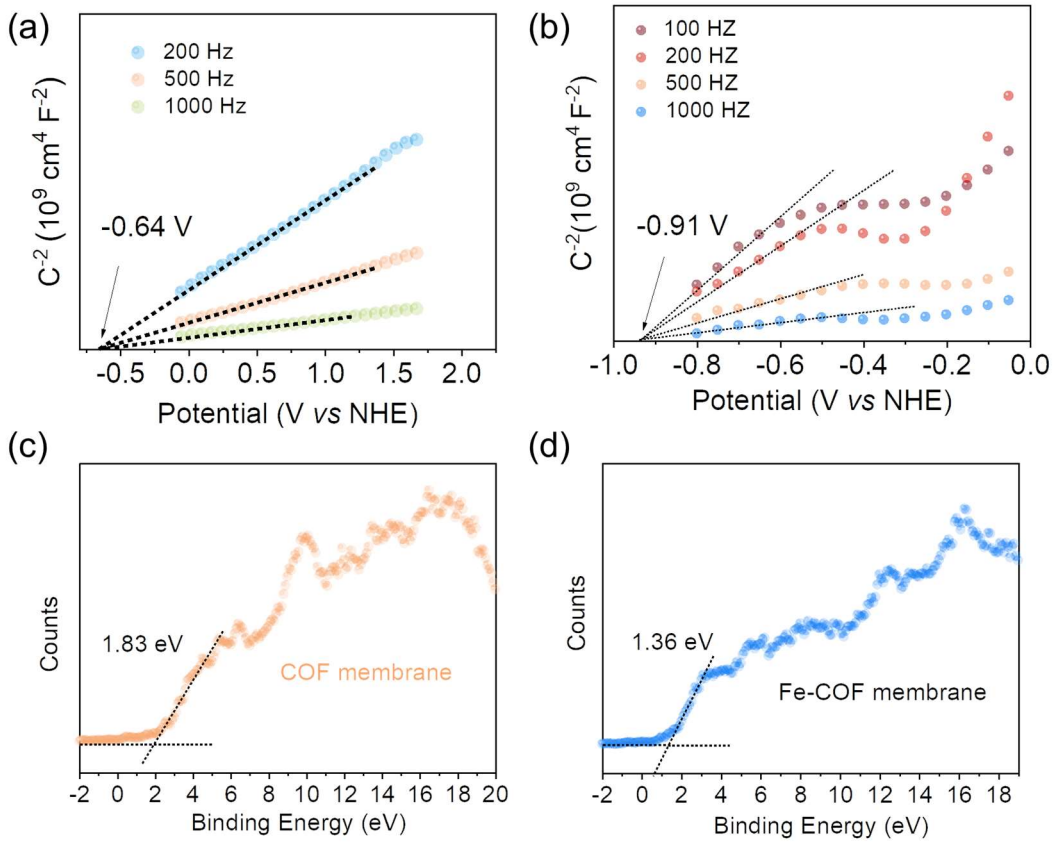

Fig. S10. Conduction band (CB) measurements via Mott-Schottky plots for (a) COF membrane and (b) Fe-COF membrane. High-resolution valence band (VB) XPS spectra of (c) COF membrane and (d) Fe-COF membrane.

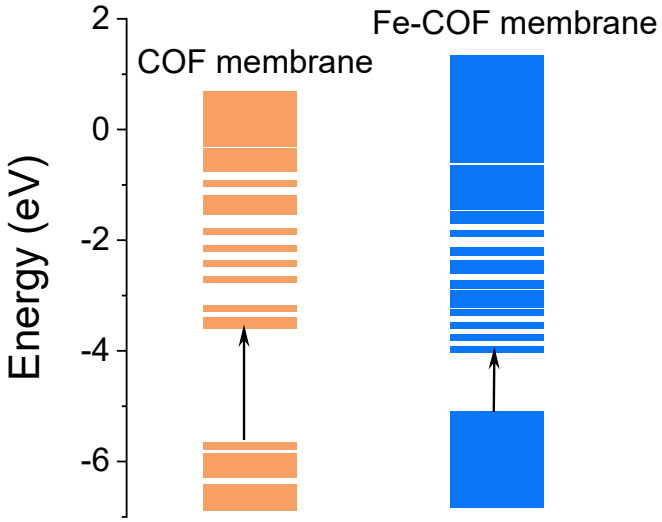

Fig. S11. DFT band gap of different COF memrbanes.

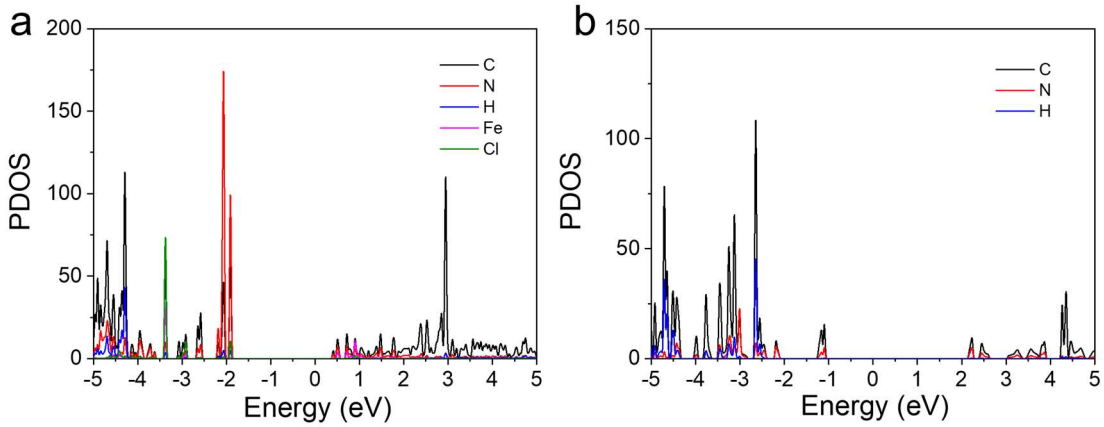

Fig. S12. PDOS of (a) Fe-COF membrane, and (b) COF membrane.

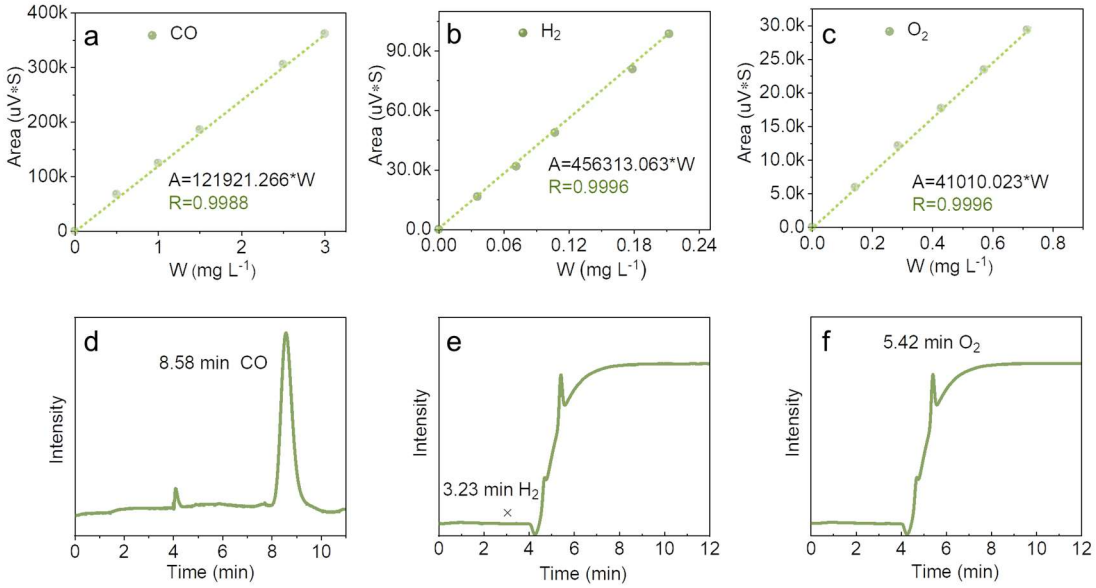

Fig. S13. Linear GC calibration plots for (a) CO, (b) H_2, and (c) O_2 spices. The peak time of (d) CO, (e) H_2, and (f) O_2 according to the GC profile of the Fe-COF membrane.

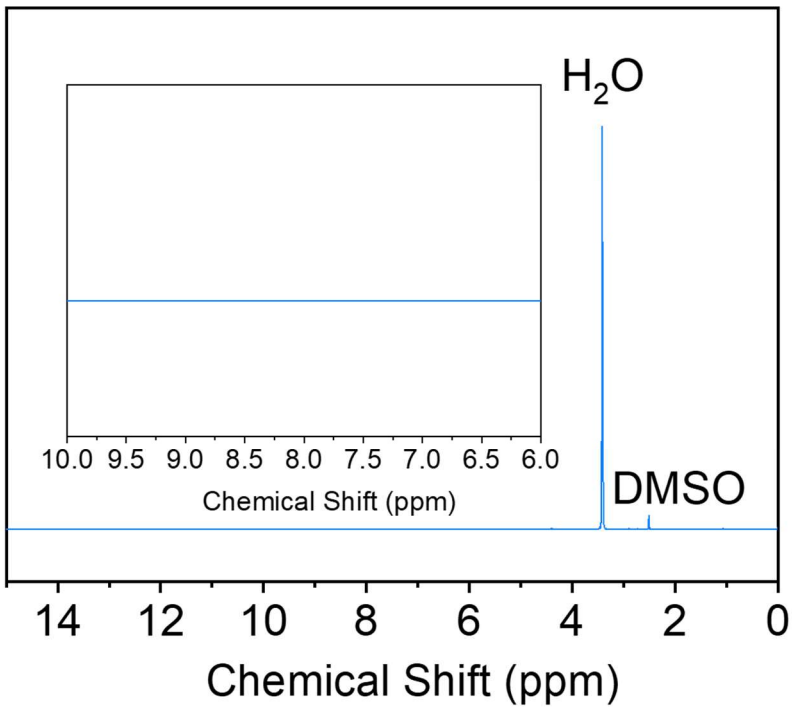

Fig. S14. ^{1}H NMR spectrum of the liquid phase product in the reactor after a 4 h CO_2 photoreduction reaction using Fe-COF membrane as the catalyst.

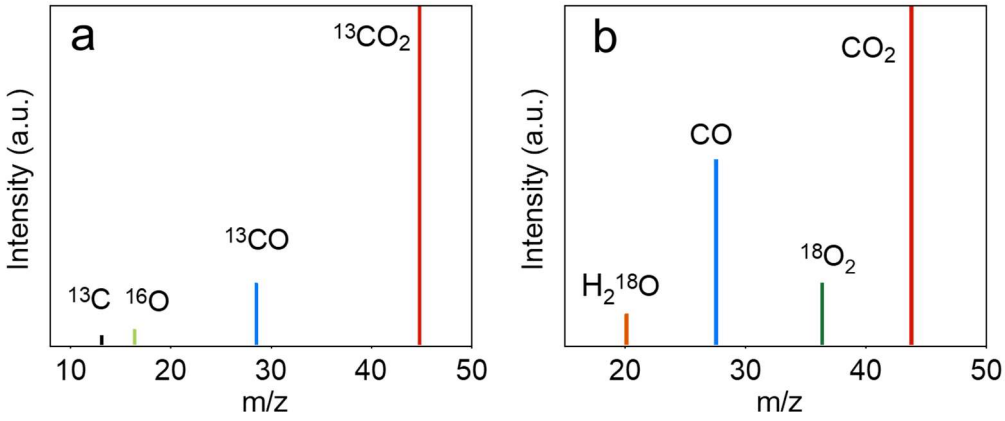

Fig. S15. (a) ^{13}C isotope tracer results and (b) ^{18}O isotope tracer results based on GC-MS for Fe-COF membrane.

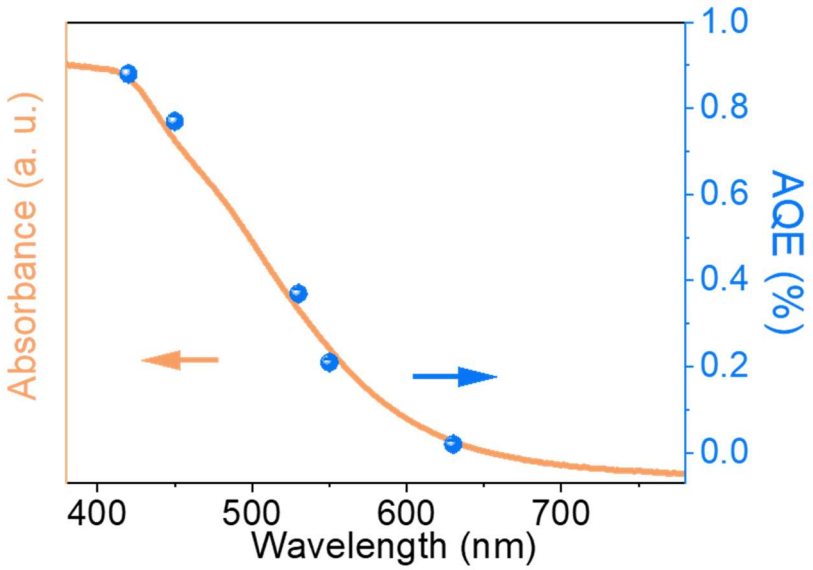

Fig. S16. AQE of the Fe-COF memrbane and the related absorption spectrum as a function of absorption wavelength.

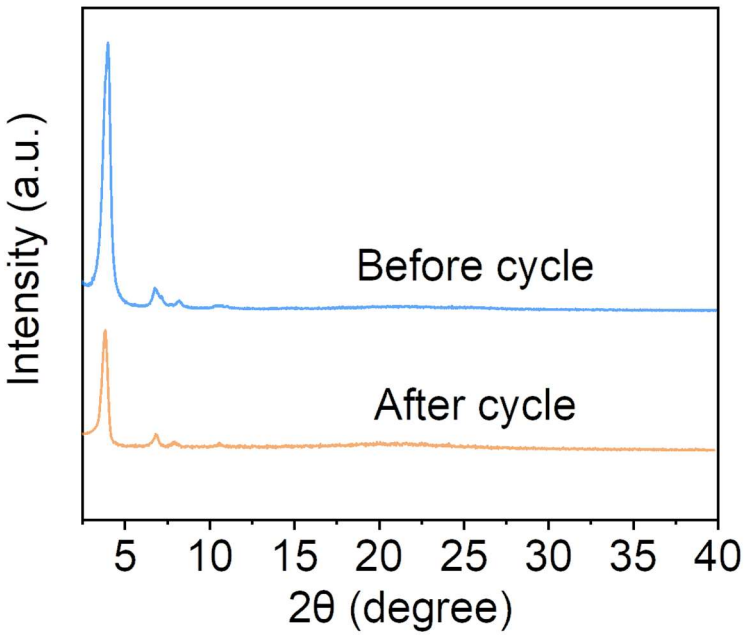

Fig. S17. XRD patterns of the Fe-COF membrane before and after the long-term stability tests.

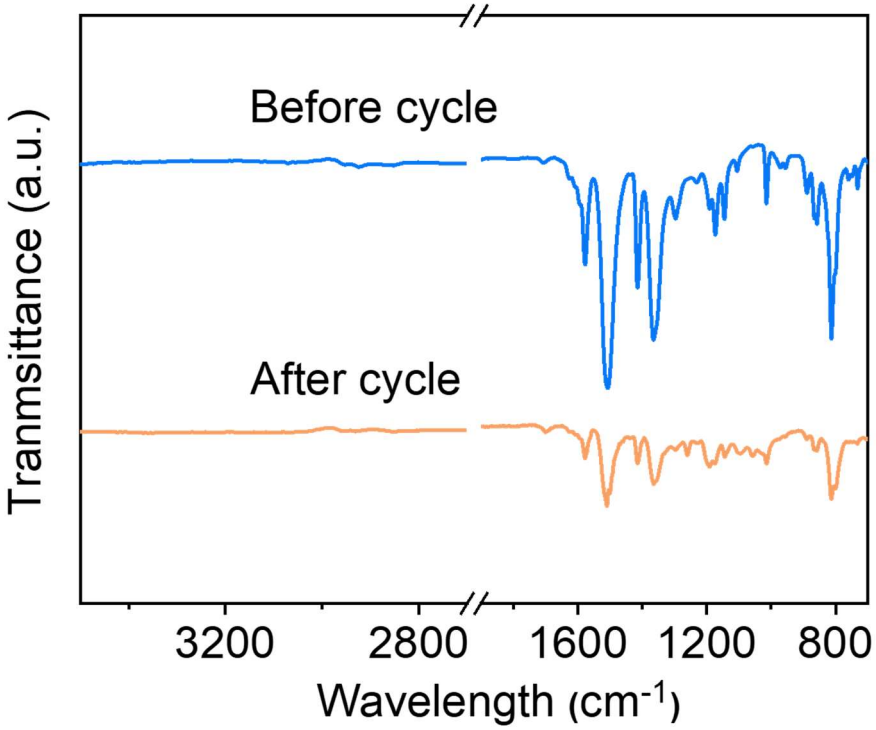

Fig. S18. FT-IR spectra of the Fe-COF membrane before and after the long-term stability tests.

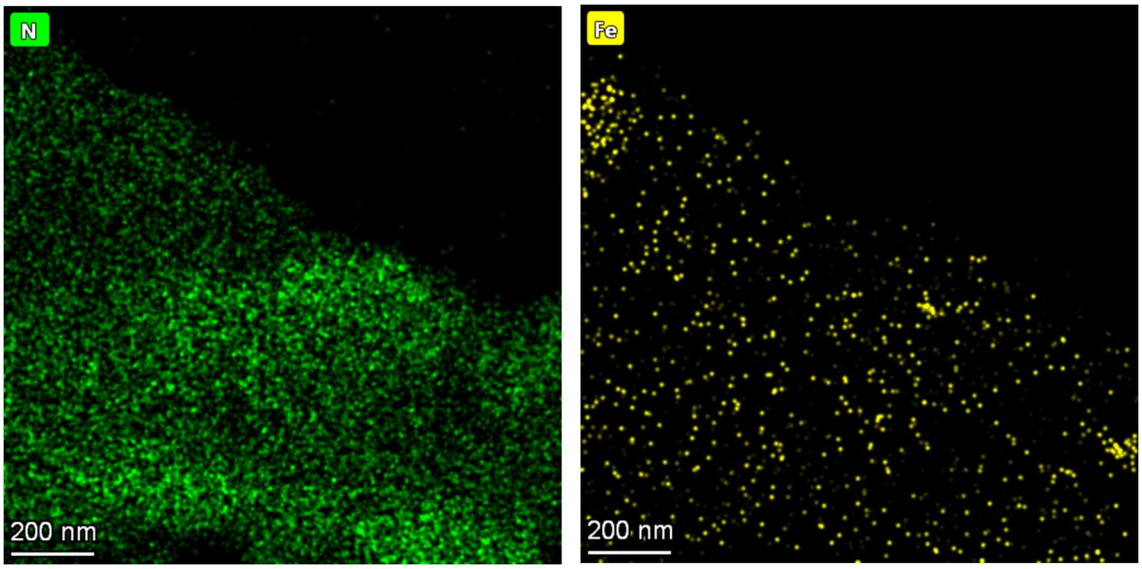

Fig. S19. The N and Fe Element mapping of the Fe-COF membrane after the long-term stability tests.

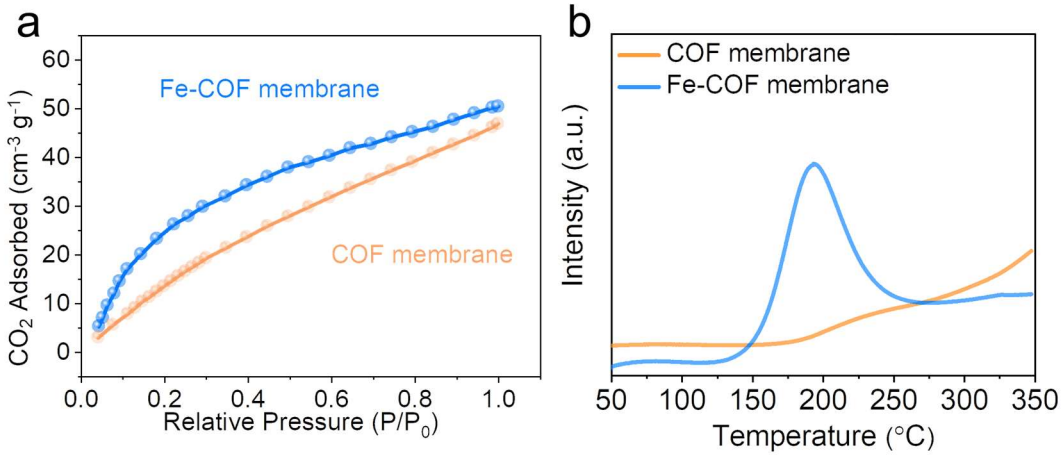

Fig. S20. (a) CO_2 adsorption capacity of different COF membranes. (b) CO_2 temperature-programmed desorption curve (CO_2-TPD).

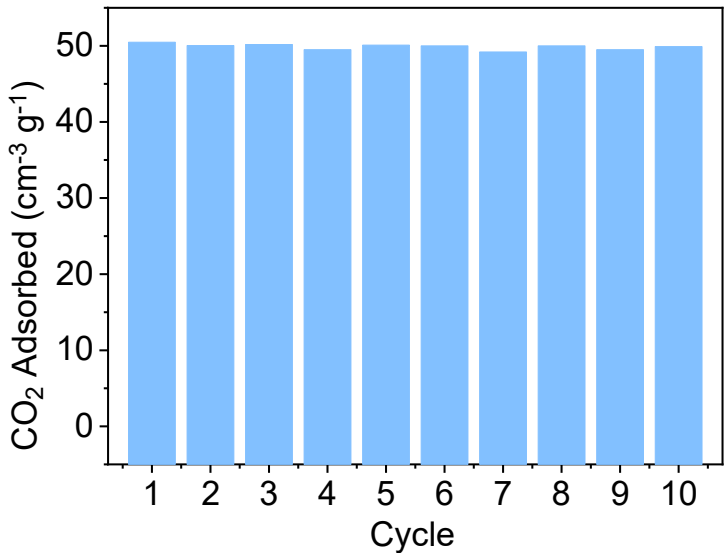

Fig. S21. CO_2 adsorption capacity of the reused Fe-COF membrane.

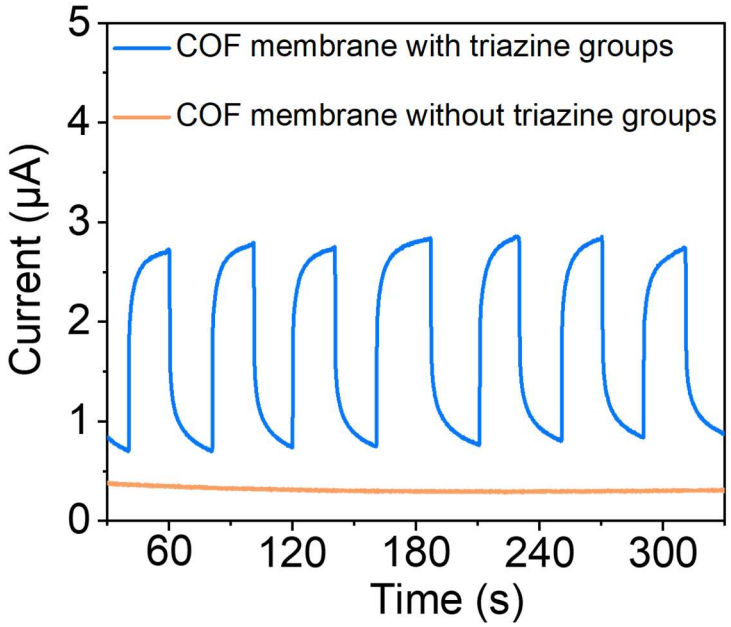

Fig. S22. Photocurrent density of the COF membranes with and without triazine groups.

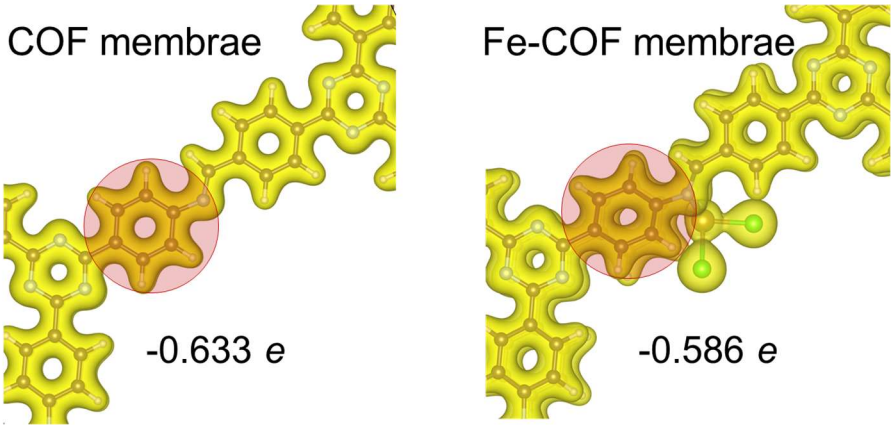

Fig. S23. The electron denisty distribution, as well as Bader charge analysis of benzene rings in pristine COF and Fe-COF membranes.

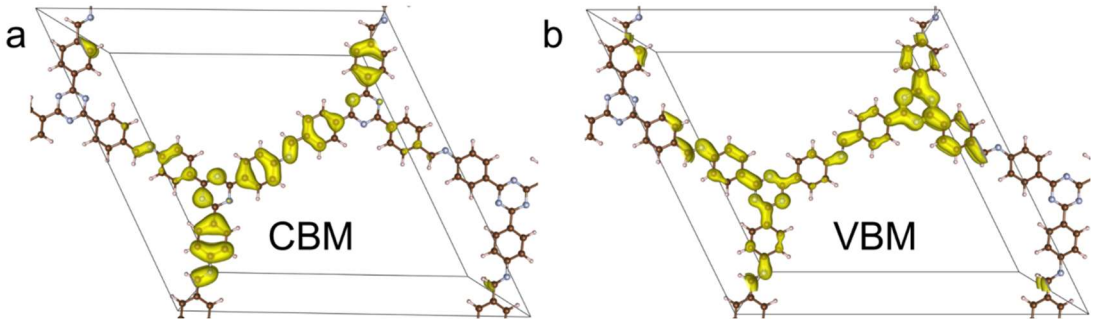

Fig. S24. (a) CBM and (b) VBM of the COF membrane.

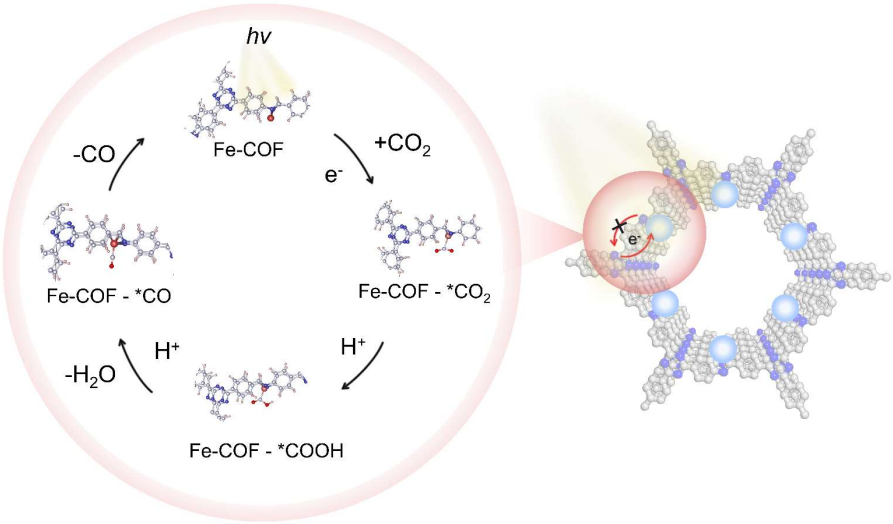

Fig. S25. Proposed reaction mechanism for photocatalytic CO_2 to CO conversion over Fe-COF membrane.

4. Tables S1-S4

Table S1. Structural parameters of the Fe-COF membrane obtained from EXAFS fitting

Sample	Shell	CN	R(Å)	σ^2(Å^2)	ΔE_0(eV)	*R factor*
Fe-COF	Fe-N	2	1.90 ± 0.05	0.0049 ± 0.008	2.84 ± 2.96	0.01
	Fe-Cl	2	2.16 ± 0.03	0.0287 ± 0.008	-14.1 ± 4.3	

CN = coordination number, R = interatomic distance (the bond length between central atoms and surrounding coordination atoms) based on fitting results, ΔE_0 = inner potential correction, σ^2 = Debye-Waller factor, and the *R factor* is used to value the goodness of fit.

Table S2. Comparison of CO evolution rate with other photocatalysts under gas-solid phase reactions (without the use of photosensitizers, sacrificial agents and cocatalysts)

Sample	Reaction condition	CO evolution rate ($\mu mol\ h^{-1}\ g^{-1}$)	Selectivity (%)	Ref
LaNi-COF-5	gas-solid system 300 W Xenon lamp	608	~98.2	[4]
TCOF-$MnMo_6$	gas-solid system 300 W Xenon lamp (≥420 nm)	37.25	~100	[5]
Bi-TTCOF-Zn	gas-solid system 300 W Xenon lamp (≥420 nm)	11.56	~100	[6]
COF-318-TiO_2	gas-solid system 300 W Xenon lamp	69.67	~100	[7]
CT-COF	gas-solid system 300 W Xenon lamp (≥420 nm)	102.7	~100	[8]
2,3-DhaTph CONs	gas-solid system 300 W Xenon lamp (≥420 nm)	132.2	~100	[9]
[Emim]BF_4 (56.41 wt%) @Zn-S-COF	gas-solid system 300 W Xenon lamp (≥420 nm)	267.9	~100	[10]
viCOF-bpy-Re	gas-solid system 300 W Xenon lamp (≥420 nm)	196	~100	[11]
OH-COF/Re-CP	gas-solid system 300 W Xenon lamp (≥420 nm)	216.2	~100	[12]
Fe-COF membrane	**gas-solid system 300 W Xenon lamp**	**993**	**~100**	**This work**

Table S3. Apparent quantum efficiency of the Fe-COF membrane at different wavelengths

Wavelengths (nm)	AQE (%)
420	0.87
450	0.76
530	0.38
550	0.21
630	0.02

Table S4. Average temperature and light intensity under the natural sunlight condition

Day	Temperature (°C)	Light intensity (mW cm^{-2})
1	22	44.5
2	24	45.1
3	25	46.7

6. References

[1]. Yao K.; Lu W.; Li X.; Wang J. Tailoring the Properties of Aqueous–Ionic Liquid Interfaces for Tunable Synthesis and Self-Assembly of ZnS Nanoparticles. *J. Mater. Chem. A* **2014**, 14, 5140-5148.

[2]. Jiang, Z.; Xu, X.; Ma, Y.; Cho, H. S.; Ding, D.; Wang, C.; Wu, J.; Oleynikov, P.; Jia, M.; Cheng, J.; et al. Filling Metal–Organic Framework Mesopores with TiO_2 for CO_2 Photoreduction. *Nature* **2020**. 586, 549-554.

[3]. Lam, E.; Reisner, E. TiO_2-Co(terpyridine)$_2$ Potocatalyst for the Selective Oxidation of Cellulose to Formate Coupled to the Reduction of CO_2 to Syngas. *Angew. Chem. Int. Ed.* **2021**, 60, 23306-23312.

[4]. Zhou, M., Wang, Z., Mei, A., Yang, Z., Chen, W., et al. Photocatalytic CO_2 reduction using La-Ni bimetallic sites within a covalent organic framework, *Nat. Commun.* **2023**, 14, 2473.

[5]. Lu, M; Zhang, M.; Liu, J.; Yu, T.; Chang, J.; Shang, L.; Jiang, D.; Zhu, X.; Popovs, I.; Lan, Y. Confining and Highly Dispersing Single Polyoxometalate Clusters in Covalent Organic Frameworks by Covalent Linkages for CO_2 Photoreduction. *J. Am. Chem. Soc.* ***2022***, 144, 1861–187

[6]. Li, Q., Chang, J., Wang, Z., Lu, M., Guo, C., Zhang, M., Yu, T., Chen, Y., Li, S., Lan, Y. Modulated Connection Modes of Redox Units in Molecular Junction Covalent Organic Frameworks for Artificial Photosynthetic Overall Reaction. *J. Am. Chem. Soc.* **2023**, 145, 23167-23175.

[7]. Hu, J.; Chen, D.; Mo, Z.; Li, N.; Xu, Q.; Li, H.; He, J.; Xu, H.; Lu, J. Semiconductor/Covalent-Organic-Framework Z-Scheme Heterojunctions for Artificial Photosynthesis *Angew. Chem. Int. Ed.* **2020**, 59, 6500-6506.

[8]. Lei, K.; Wang, D.; Ye, L.; Kou, M.; Deng, Y.; Ma, Z.; Wang, L.; Kong, Y. A Metal-Free Donor-Acceptor Covalent Organic Framework Photocatalyst for Visible-Light-Driven Reduction of CO_2 with H_2O. *ChemSusChem* **2022**, 13, 1725-1729.

[9]. Guo, Y.; Zhang, Q.; Gao, S.; Wang, H.; Li, Z.; Qiu, J.; Zhao, Y.; Liu, Z.; Wang, J. Bi-Functional Ionic Liquids Facilitate Liquid-Phase Exfoliation of Porphyrin-

Based Covalent Organic Frameworks in Water for Highly Efficient CO_2 Photoreduction. *Green Chem.* **2022**, 24, 9530-9541.

[10]. Yang, Y.; Zhang, H.; Wang, Y.; Shao, L.; Fang, L.; Dong, H.; Lu, M.; Dong, L.; Lan, Y.; Zhang, F. Integrating Enrichment, Reduction, and Oxidation Sites in One System for Artificial Photosynthetic Diluted CO_2 Reduction. *Adv. Mater.* **2023**, 35, 2304170.

[11]. Cheng, Y.; Ji, W.; Hao, P.; Qi, X.; Wu, X.; Dou, X.; Bian, X.; Jiang, D.; Li, F.; Liu, X.; Yang, D.; Ding, X.; Han, B. A Fully Conjugated Covalent Organic Framework with Oxidative and Reductive Sites for Photocatalytic Carbon Dioxide Reduction with Water. *Angew. Chem. Int. Ed.* **2023**, 62, e202308523.

.

[12]. Wang, Y.; He, H.; Li, Y.; Wang, W.; Deng, L.; Wu, L.; Zhang, Y.; Huang, J.; Zhang, P.; Yu, J.; Liu, Y. Unraveling the photo-induced dynamic behavior of COF-based Z-scheme heterostructure monolithic aerogels. *Matter.* **2024**, 7, 3145-3162.